ALDH5A1 as a key in osteonecrosis of the femoral head: Insights from bioinformatics and experimental validation

TIANYU REN, QINGFA QIN, LI PANG, XIFAN ZHENG, JUNPU HUANG, JINZHI MENG, YUE QIU, ZEMING LI and JUN YAO

Department of Bone and Joint Surgery, The First Affiliated Hospital of Guangxi Medical University, Nanning, Guangxi Zhuang Autonomous Region 530021, P.R. China

Received August 17, 2025; Accepted February 13, 2026

DOI: 10.3892/br.2026.2136

Abstract. The present study aims to identify key genes and elucidate the molecular mechanisms underlying osteonecrosis of the femoral head (ONFH), with the goal of discovering effective diagnostic and therapeutic targets. Microarray data were sourced from the Gene Expression Omnibus database. Differentially expressed genes (DEGs) were identified using the Limma method. Feature genes were selected through Support Vector Machine, Random Forest and Least Absolute Shrinkage and Selection Operator algorithms. Diagnostic performance was assessed using receiver operating characteristic (ROC) analysis. Functional enrichment and immune infiltration analyses were performed. Experimental validation included RT-qPCR, western blotting and immunofluorescence in ONFH bone tissue. Additionally, a competing endogenous RNA (ceRNA) network was constructed using Cytoscape (v3.10.1). A total of 51 DEGs were identified, comprising 33 downregulated and 18 upregulated genes. Aldehyde dehydrogenase 5 family member A1 (ALDH5A1) consistently emerged as a key gene across all machine learning models, demonstrating high diagnostic value according to ROC analysis. Enrichment analysis indicated that ALDH5A1-related DEGs were predominantly involved in 'Toll-like receptor signaling', 'RIG-like receptor signaling', 'Leishmania infection' and 'Cytosolic DNA sensing'. Immune analysis revealed associations between ONFH and HLA/MHC-I molecules, neutrophils and regulatory T cells, with ALDH5A1 showing a negative correlation with activated $CD4^+$ memory T cells. Experimental validation confirmed significant downregulation of ALDH5A1 in ONFH samples. Overall, ALDH5A1 represents a promising prognostic biomarker and potential therapeutic target for ONFH. The interaction between immune cells and the ceRNA network may play a critical role in the pathogenesis of ONFH, providing valuable insights for molecular mechanisms and clinical intervention strategies.

Correspondence to: Professor Jun Yao, Department of Bone and Joint Surgery, The First Affiliated Hospital of Guangxi Medical University, 6 Shuangyong Road, Qingxiu, Nanning, Guangxi Zhuang Autonomous Region 530021, P.R. China
E-mail: yaojun800524@126.com

Key words: femoral head, osteonecrosis, diagnostic biomarkers, machine learning, competing endogenous RNA networks, immune cell infiltration

Introduction

Osteonecrosis of the Femoral Head (ONFH) is a prevalent clinical condition characterized by the degeneration of subchondral bone, leading to severe hip pain and substantial functional impairment (1,2). The disease is multifactorial, with the primary cause being disruption of blood supply to the femoral head, resulting in the death of bone cells, subsequent collapse of the femoral head, and degenerative changes in the hip joint. While corticosteroid use, alcohol consumption, sickle cell disease, and trauma are well-established risk factors for ONFH, the precise mechanisms underlying its pathogenesis remain unclear (3,4). Treatment options for early-stage ONFH range from surgical procedures aimed at preserving hip function to pharmacological therapies (5,6). However, most patients ultimately require total hip arthroplasty, which remains the most effective treatment (7,8). Moreover, many young patients face the need for revision surgeries, exacerbating the socioeconomic burden. Consequently, there is an urgent need to identify novel biomarkers and therapeutic targets, which are crucial for early diagnosis and the development of new treatment strategies for ONFH.

Recent research has increasingly focused on the role of biomolecules in ONFH pathogenesis. For instance, Yu *et al* demonstrated the significant influence of immune cell infiltration on ONFH onset and progression, highlighting a close correlation with specific immune cell subpopulations (9). Fang *et al* identified that immune and m6A regulatory factors play pivotal roles in mediating the inflammatory response in ONFH, particularly involving Th2-dominated immune cells and inflammatory mediators (10). However, the detailed pathological processes remain incompletely understood. Additionally, gene chips and high-throughput sequencing technologies have proven valuable for identifying pathogenic genes, providing reliable and actionable insights (11). Thus, investigating novel molecular markers and immune cell

infiltration in ONFH is critical for elucidating its underlying pathogenic mechanisms.

This study integrated microarray datasets from the Gene Expression Omnibus (GEO) database with cartilage samples from patients with ONFH and supplemented these with our own microarray data derived from subchondral bone samples of ONFH individuals. Using machine learning techniques, this study identified key genes, validated them via ROC analysis, and compared immune cell infiltration across 22 immune cell subtypes in ONFH and healthy controls using the CIBERSORT algorithm. This study further identified key molecular pathways and functional networks within ONFH tissues, employing bioinformatics analysis to elucidate the roles of differentially expressed mRNAs. Ultimately, critical feature genes were identified as molecular markers for both ONFH diagnosis and immune infiltration.

Materials and methods

Obtaining and handling data. The GEO database (http://www.ncbi.nlm.nih.gov/geo/) was utilized to download experimental group files for GSE74089 and GSE123568. The dataset, consisting of 14 normal synovial tissue samples (labeled as 'normal') and 34 ONFH synovial tissue samples (labeled as 'ONFH'), was processed using the limma package in R software (version 3.58.1) for data correction and normalization. The samples were divided into two groups: the ONFH group (designated as 'Treatment') and the normal group (designated as 'Control'). Additionally, GSE178557, which included four samples each of ONFH and normal synovial tissue, was used as an independent validation dataset for external verification.

Identification of DEGs and characteristic genes. To identify differentially expressed genes (DEGs), a multi-step approach was employed. The limma package in R (version 3.58.1) was used to filter DEGs from all datasets, applying the criteria of logFC >1 and an adjusted P-value <0.05. Following DEG screening, feature genes were selected using Lasso regression, with the glmnet (version 4.1-7) and e1071 (version 1.7-14) packages. Additionally, the Support Vector Machine (SVM) algorithm, implemented via the e1071 package (version 1.7-14), was applied to DEGs to identify another set of feature genes. Finally, Random Forest (RF) analysis was conducted on the DEGs using ggplot2 software, and genes with a gene importance score greater than 2 (rfGenes >2) were selected. By intersecting the characteristic genes identified by these three methods, a final subset of significant genes was obtained. One of these genes was chosen for further investigation as a potential marker gene.

Evaluate the accuracy of characteristic genes. A violin plot was generated using the ggpubr package (version 0.6.0) to visualize the expression differences of the selected feature genes between the ONFH (treatment) and normal (control) groups.

Statistical significance was determined with P<0.05. The discriminative ability of the identified feature genes in distinguishing normal from ONFH samples was assessed through Receiver Operating Characteristic (ROC) curve analysis using the pROC package. The accuracy of the ROC curve was measured by calculating the area under the curve (AUC), with an AUC value greater than 0.7 considered indicative of satisfactory performance. Finally, ROC curve analysis and differential expression analysis were performed on the validation group samples to confirm the validity of the experimental group findings.

Analysis of the correlation of signature genes. After identifying the disease-related signature gene through the established screening criteria, samples were classified into high and low expression groups based on the signature gene expression levels using the limma package (version: 3.58.1) in R. The filtering criteria were set as logFC >1 and adj.P.Val <0.05. DEGs associated with the signature gene were identified through correlation analysis, with genes exhibiting a strong correlation selected for further analysis. Data visualization was performed using heatmaps and volcano plots, while gene correlations were illustrated through correlation bubbles generated using the corrplot package.

Functional enrichment analysis. Kyoto Encyclopedia of Genes and Genomes (KEGG) pathway enrichment analysis was performed to identify significantly enriched pathways (https://www.kegg.jp/). To explore the functional enrichment of DEGs linked to the signature gene, Gene Ontology (GO) enrichment analyses were performed, focusing on biological processes (BPs), cellular components (CCs), and molecular functions (MFs). Gene Set Enrichment Analysis (GSEA) was performed to assess the enrichment and scoring values for the high and low expression groups of the signature gene, providing insights into their significance in relevant biological processes and functions.

Immune cell infiltration and correlation analysis. R software was employed to analyze immune molecular functions in ONFH and normal group samples, identifying significant differences between the two groups. Immune cell infiltration was assessed using the CIBERSORT tool, which applied an inverse convolution technique to estimate the proportions of 22 lymphocyte subpopulations across tissue samples (12). Following immune cell infiltration analysis, the relationship between immune infiltrating cells and gene expression was investigated using the Spearman correlation algorithm with a significance threshold of P<0.05. This correlation analysis aimed to determine the associations between characteristic genes and immune cell infiltration, with the results presented in graphical format.

Investigation of the signature gene's RNA network. To predict the regulatory relationships between miRNAs and the signature gene, TargetScan (https://www.targetscan.org/) (13), miRanda (http://mirtoolsgallery.tech/mirtoolsgallery/) (14), and miRDB (https://mirdb.org/) (15) were used. In TargetScan, a Context score percentile cutoff of ≥90 was applied, and in miRDB, the Target Score cutoff was set at ≥90. The Director package (version: 3.1.9) was downloaded from the miRanda database to obtain the top 1% ranked genes. These results were consolidated for further analysis. Additionally, the spongeScan database was utilized to identify long non-coding

RNAs (lncRNAs) that may compete with miRNAs for binding *via* microRNA response elements (MREs). Finally, the ceRNA regulatory network, consisting of the signature gene, miRNAs, and lncRNAs, was visualized using Cytoscape v3.10.1.

Isolation and cultivation of chondrocytes. Synovial cartilage samples were collected from patients diagnosed with traumatic femoral neck fractures and severe femoral head necrosis who underwent joint replacement surgery at the First Affiliated Hospital of Guangxi Medical University between January 2021 and December 2023. The study included a control group of 6 patients with femoral neck fractures (5 males and 1 female) and an experimental group of 6 patients with severe femoral head necrosis (4 males and 2 females). All procedures were approved by the Medical Ethics Committee of the First Affiliated Hospital of Guangxi Medical University (Ethical approval no. 2021-E67-01).

Immediately after surgery, femoral head cartilage samples were stored at -80˚C for subsequent processing. Approximately 100 g of femoral head cartilage was excised from each patient, cut into small pieces, and subjected to enzymatic digestion using trypsin and type I collagenase. The released chondrocytes were harvested and cultured in high-glucose Dulbecco's Modified Eagle Medium (DMEM) supplemented with 10% fetal bovine serum and antibiotics. The cells were maintained at 37˚C in a humidified incubator with 5% CO_2. Chondrocytes from passage 3 were used for all subsequent experiments.

RNA extraction, cDNA synthesis, and quantitative PCR. Synovial cartilage samples were obtained from patients with ONFH and normal femoral head cartilage. Total RNA was extracted from approximately 50 g of cartilage tissue using the RNAeasy™ Plus Animal RNA Isolation Kit (Beyotime Biotechnology), following the manufacturer's instructions. A total of 1 μg of RNA was reverse-transcribed into complementary DNA (cDNA) using the PrimeScript™ RT Reagent Kit with gDNA Eraser (Takara).

Quantitative real-time PCR (qRT-PCR) was performed to assess ALDH5A1 mRNA expression levels in both ONFH and normal femoral head cartilage. Gene-specific primers were designed based on GenBank sequences. The qRT-PCR reaction consisted of 0.5 μl of each primer, 1.5 μl of distilled water, 2.5 μl of cDNA, and 5 μl of SYBR Premix Ex Taq mix (Thermo Fisher Scientific, Inc.), making up a final volume of 10 μl. GAPDH was used as the internal control, and relative expression levels of ALDH5A1 were calculated using the $2^{-\Delta\Delta Ct}$ method. All experiments were conducted in triplicate.

Primer sequences were as follows: ALDH5A1, forward, 5'-ATCACCCCGTGGAATTTCCC-3'; reverse, 5'-TTCACC ACGACAGTACAGCC-3'. GAPDH, forward, 5'-CACCCA CTCCTCCACCTTTGAC-3'; reverse, 5'-GTCCACCACCCT GTTGCTGTAG-3'.

Protein extraction and western blotting. Total protein was extracted from femoral head cartilage using RIPA buffer containing PMSF (BOSTER), phosphatase inhibitors (CWBIO), and protease inhibitors (MCE). Protein concentration was determined using the BCA assay (Beyotime Biotechnology) following the manufacturer's instructions.

Protein samples were mixed with loading buffer and heated at 100˚C for 10 min. Proteins were separated by SDS-PAGE (10% polyacrylamide gel) and transferred to PVDF membranes. Membranes were blocked with 5% skim milk for 2 h at room temperature, followed by overnight incubation at -4˚C with primary antibodies against ALDH5A1 and GAPDH (Proteintech) at a 1:5,000 dilution. After washing with PBST, membranes were incubated for 1 h at room temperature with a rabbit anti-rat IgG secondary antibody. Protein signals were detected using an Odyssey infrared imaging system, and chemiluminescence was visualized using enhanced chemiluminescence (Beyotime Biotechnology).

Immunofluorescence staining. Chondrocytes were cultured overnight on sterile glass coverslips at 37˚C with 5% CO_2. Cells were fixed with 4% paraformaldehyde for 15 min, permeabilized with permeabilization solution (Beyotime Biotechnology) for 10 min, and blocked with immunofluorescence blocking buffer (Beyotime Biotechnology) for 1 h at room temperature. After washing, cells were incubated overnight at 4˚C with anti-ALDH5A1 primary antibody (Proteintech, China), followed by 2-h incubation with FITC-conjugated goat anti-rabbit IgG secondary antibody (Epizyme Biotech, China) in the dark. Nuclei were stained with DAPI (1 μg/ml) for 10 min. Images were captured using a Revolve2 inverted fluorescence microscope (Echo), and fluorescence intensity was quantified using ImageJ software.

Statistical analyses. Bioinformatics analysis was performed using R (x64 4.3.1). For the *in vitro* experiment, data were analyzed with GraphPad Prism 8.0.2 and ImageJ and are presented as mean ± standard error. Statistical differences between groups were evaluated using an unpaired Student's t-test, with $P<0.05$ considered statistically significant.

Statement. This study was approved by the Medical Ethics Committee of the First Affiliated Hospital of Guangxi Medical University (approval number: 2021-E67-01) in Guangxi, China. The handling of clinical tissue samples adhered to the ethical standards outlined in the Declaration of Helsinki.

Results

Identification of DEGs and signature genes. The limma package (version 3.58.1, Department of Mathematics and Statistics, University of Melbourne, Australia) in R software was employed to apply adjusted P-values across all datasets. Using filtering criteria of adjusted P-value <0.05 and logFC >1, 51 significant DEGs were identified, including 33 downregulated and 18 upregulated genes. The heatmap (Fig. 1A) visualizes the expression patterns of these DEGs, while the volcano plot (Fig. 1B) illustrates their differential expression levels. Furthermore, 51 DEGs were cross-validated using Lasso regression, SVM, and RF algorithms in R (Fig. 2A-C), yielding a Venn diagram (Fig. 2D) that identified three key characteristic genes: ALDH5A1, TBCEL, and KAT2B (Table I). Based on prior research, ALDH5A1 has been linked to mitochondrial dysfunction and anti-inflammatory effects (16) and was selected as a marker gene for further investigation. Basic information for ALDH5A1 was retrieved

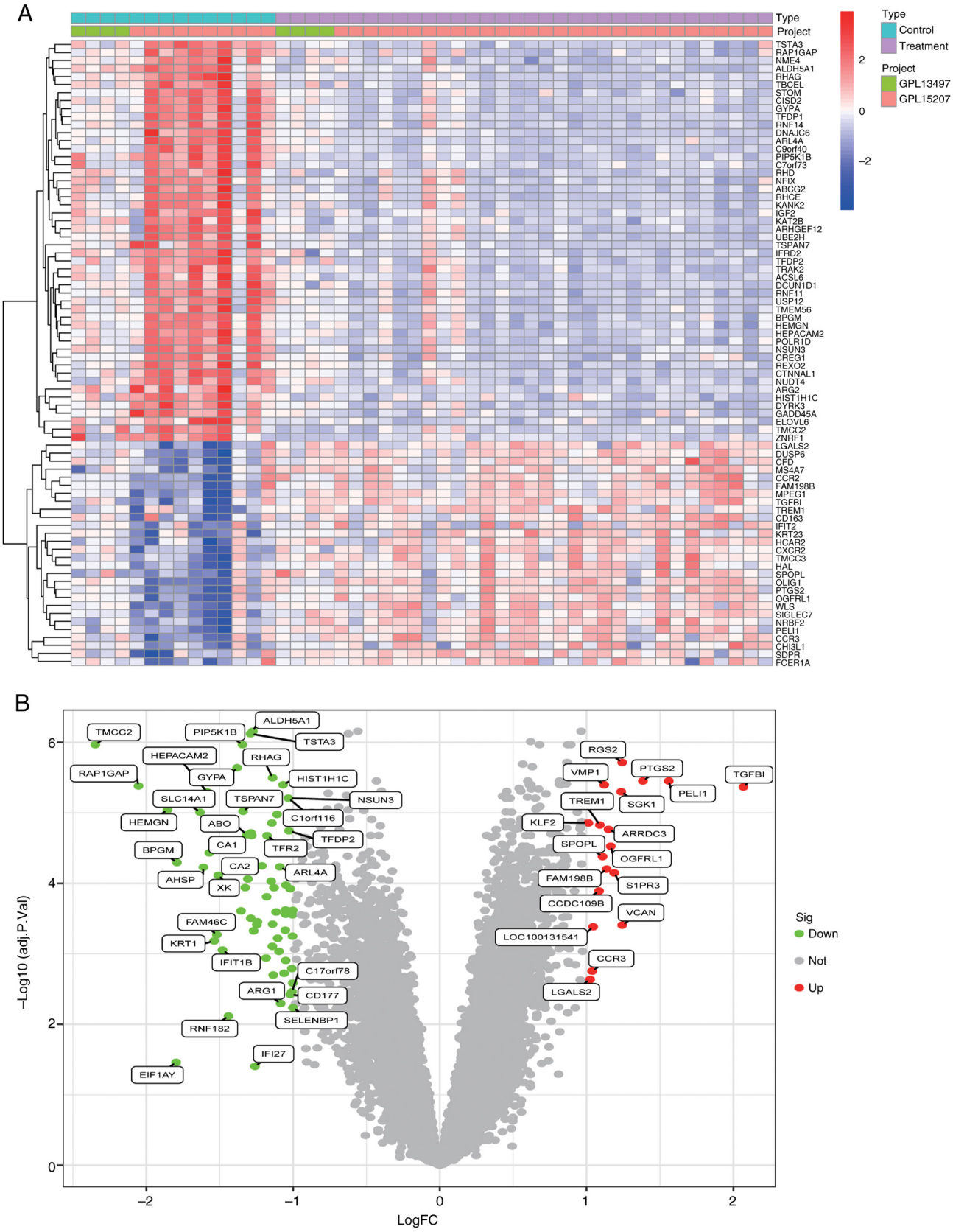

Figure 1. Identification of DEGs. (A) Heatmap of DEGs. (B) Volcano plot of DEGs. DEGs, differentially expressed genes.

from the GeneCards database (https://www.genecards.org/): Protein ID: ALDH5A1 (UniProtKB/SwissProt: P51649); Primary intracellular localization: mitochondria; Protein size: 535 amino acids; Molecular weight: 57,215 daltons.

Accuracy analysis of characteristic genes. To evaluate the discriminative ability of the three identified feature genes, ROC analysis was performed for ALDH5A1, TBCEL, and KAT2B (Fig. S1). The results indicated that all three genes possessed

Table I. Algorithms for genetic screening results.

Algorithm	Genes
LASSO	ALDH5A1, TSTA3, TMCC2, TBCEL, ARG2, KAT2B, HIST1H1C, TREM1, LTF
SVM	ALDH5A1, KAT2B, ARG2, TBCEL, YPEL4, FHDC1
RF	ALDH5A1, TBCEL, KLC3, ZNRF1, CISD2, KAT2B, USP12

LASSO, Least Absolute Shrinkage and Selection Operator; SVM, Support Vector Machine; FR, Random Forest.

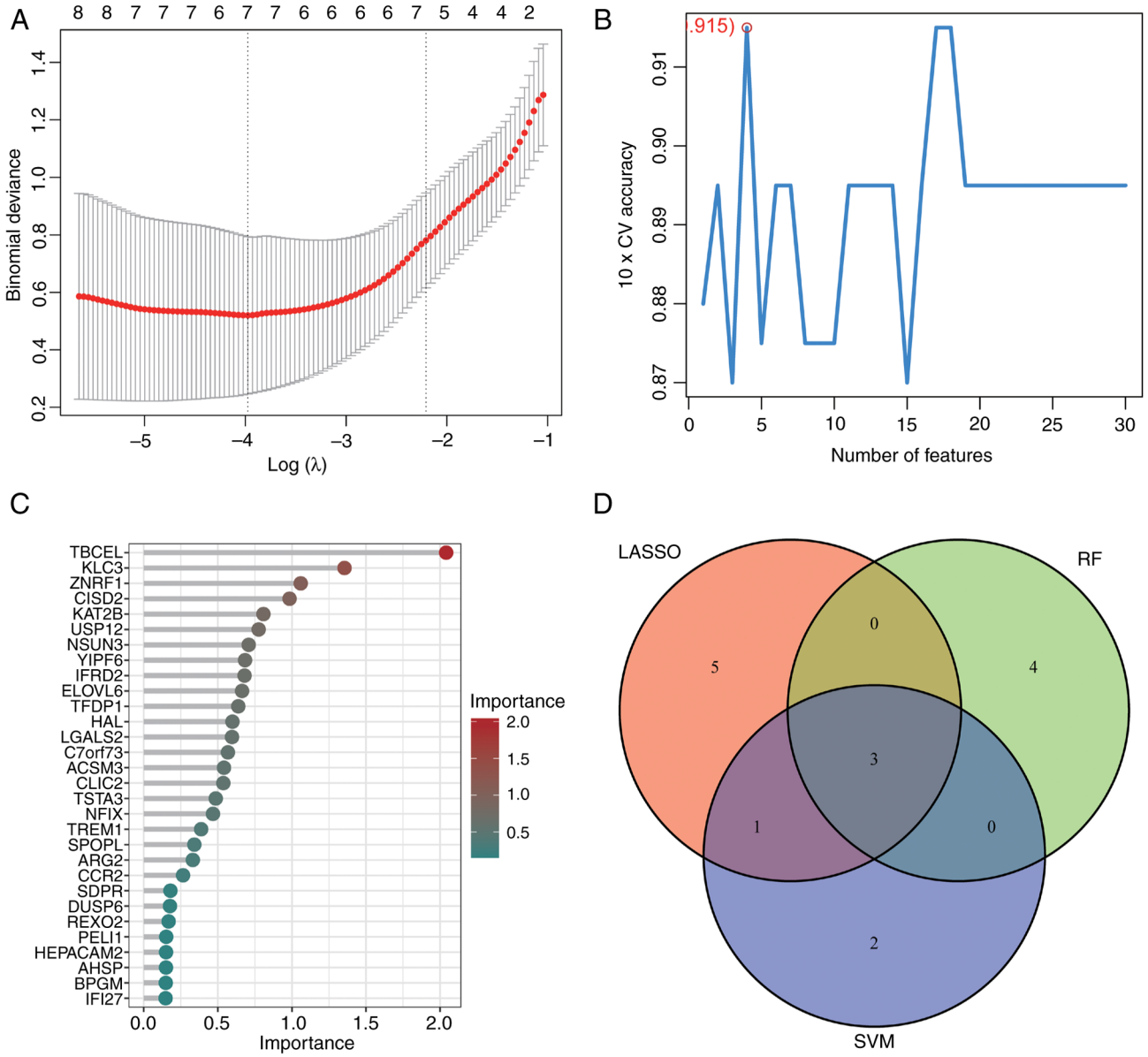

Figure 2. Identification of signature gene. (A) LASSO regression screening to obtain 9 DEGs. (B) SVM algorithm screening yielded 6 DEGs. (C) RF algorithm screening yielded 7 DEGs. (D) Venn diagram showing cross-validation yields 3 DEGs. RF, Random Forest; SVM, Support Vector Machine; LASSO, Least Absolute Shrinkage and Selection Operator; DEGs, differentially expressed genes.

robust diagnostic potential; however, ALDH5A1 exhibited the superior diagnostic accuracy with an AUC of 0.968, compared to 0.931 for TBCEL and 0.899 for KAT2B. Consequently, ALDH5A1 was selected as the optimal biomarker for further analysis. The violin plot generated using the ggpubr software (Fig. 3A) indicated that the expression level of ALDH5A1 in the ONFH group was significantly lower than in the normal group (P<0.05). Validation of these findings in the validation group was confirmed through the violin plot (Fig. 3B) and corresponding ROC curve, further supporting the reliability

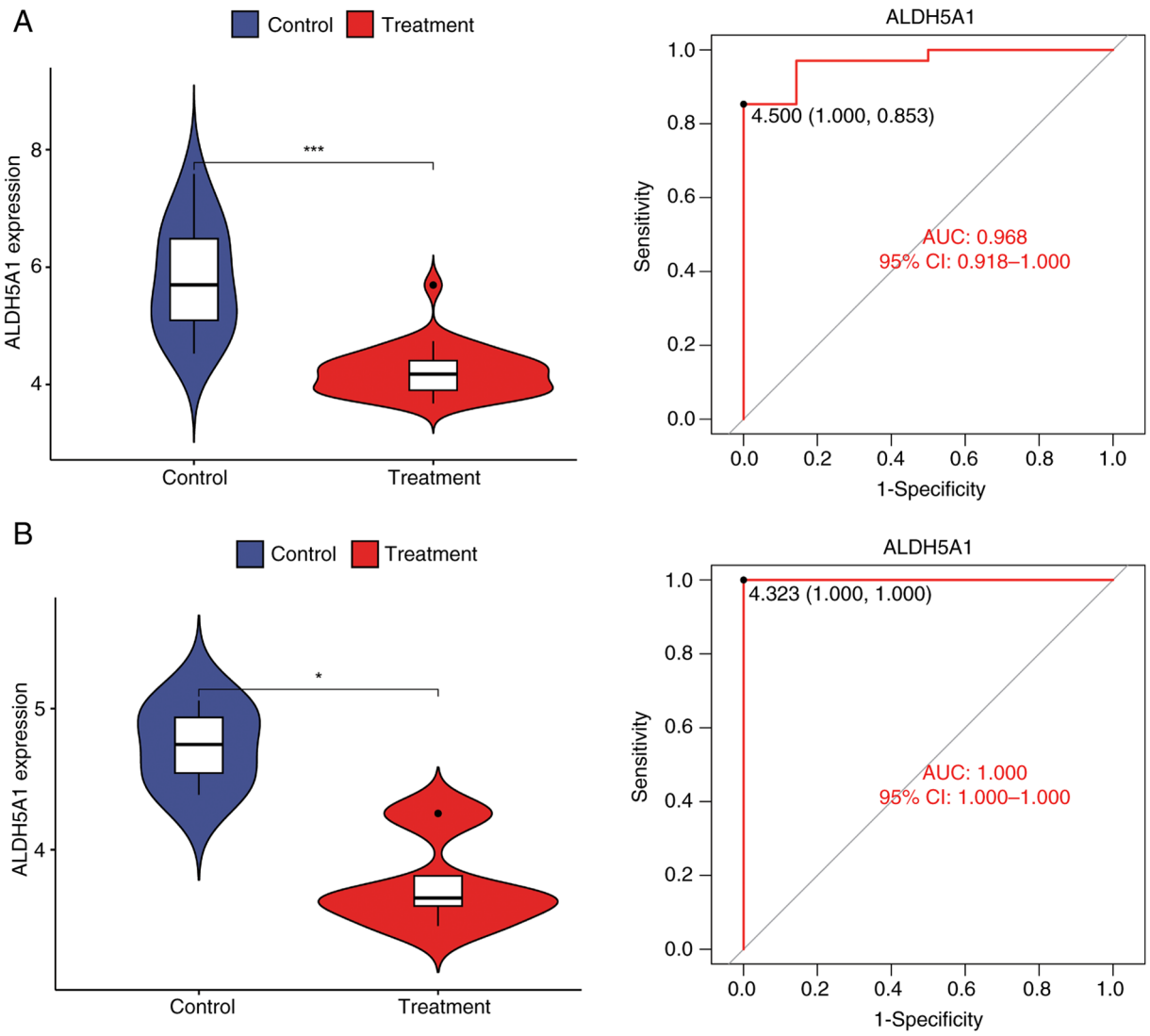

Figure 3. Accuracy analysis of signature gene. (A) Differential violin plots and ROC curves for ALDH5A1 in experimental groups. (B) Differential violin plots and ROC curves for ALDH5A1 in validation groups. *P<0.05 and ***P<0.001. ROC, receiver operating characteristic; ALDH5A1, Aldehyde dehydrogenase 5 family member A1; AUC, area under curve.

and accuracy of the ALDH5A1 marker identified in the experimental group samples.

Correlation analysis of characteristic genes. In the correlation study of ALDH5A1, as shown in the volcano map and differential heatmap (Fig. 4A and B), a correlation analysis filter identified 39 DEGs associated with ALDH5A1. Among them, 20 were upregulated and 19 were downregulated. The correlation and expression pattern of these ALDH5A1-related DEGs are depicted in the bubble plot (Fig. 4C).

Functional enrichment analysis. The results of the GO enrichment analysis are detailed in Fig. 5. The bar plot (Fig. 5A) highlights the top significant terms, showing that ALDH5A1-related DEGs are primarily enriched in biological processes such as anion transmembrane transport and regulation of autophagy. The bubble plot (Fig. 5B) complements this, displaying GeneRatio, adjusted P-values, and gene counts for these significant terms. In terms of CC, DEGs are predominantly localized in lysosomes and azurophilic granules. Regarding MF, DEGs are strongly associated with transmembrane transporter activity. These results suggest that ALDH5A1 may influence ONFH pathophysiology by participating in signal transduction pathways that regulate autophagy. According to Gene Set Variation Analysis (GSVA), upregulated genes among the DEGs related to ALDH5A1 are primarily enriched in pathways such as nitric oxide receptor signaling, Leishmania infection, TOLL-like receptor signaling, cytosolic DNA sensing, RIG-like receptor signaling, and vesicle transport. Conversely, downregulated genes are enriched in pathways associated with proximal tubular bicarbonate reclamation, nitrogen metabolism, ECM-receptor interactions, basal cell carcinoma, porphyrin and chlorophyll metabolism, and the mammalian circadian rhythm (Fig. 5C).

Gene set enrichment analysis. By classifying the experimental samples into high and low expression groups of ALDH5A1, this study further explored its biological significance in ONFH through GSEA. The high expression

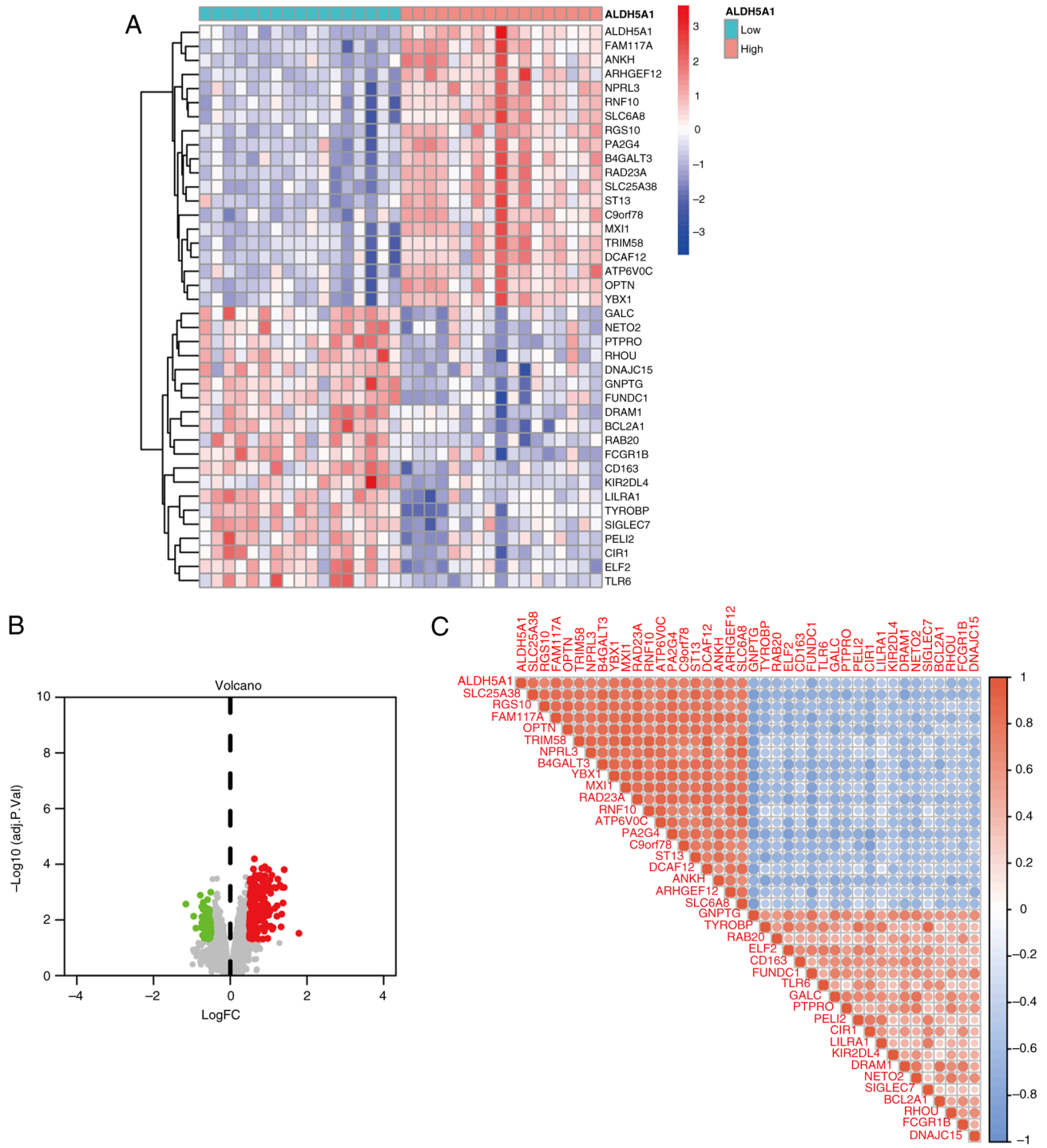

Figure 4. Signature gene correlation analysis. (A) Heatmap of ALDH5A1-related DEGs. (B) Volcano plot of ALDH5A1-related DEGs. (C) Bubble plot of ALDH5A1-related DEGs. ALDH5A1, Aldehyde dehydrogenase 5 family member A1; DEGs, differentially expressed genes.

group was significantly enriched in five activities and pathways related to lysosomal function and receptor signaling pathways (Fig. 6A). In contrast, the low expression group exhibited enrichment in five biological signaling pathways, including primary immune cell efficiency, ribosome activity, hematopoietic cell function, asthma, and autoimmune thyroid disease (Fig. 6B). These findings highlight the potential role of ALDH5A1 in regulating signal transduction and autophagy, highlighting its critical involvement in the pathogenesis of ONFH.

Correlation and immune cell infiltration analysis. Immune-related functional analysis revealed significant differences between the two ALDH5A1 expression groups in terms of HLA and MHC class I molecular functions, neutrophil and T cell co-inhibition, and regulatory T cell functions (Fig. 7). These functions were particularly active in the low ALDH5A1 expression group. Immune cell infiltration analysis, depicted in the bubble plot (Fig. 8A), shows the distribution of 22 immune cell types across the normal and ONFH groups. The volcano plot (Fig. 8B) illustrates a strong negative correlation

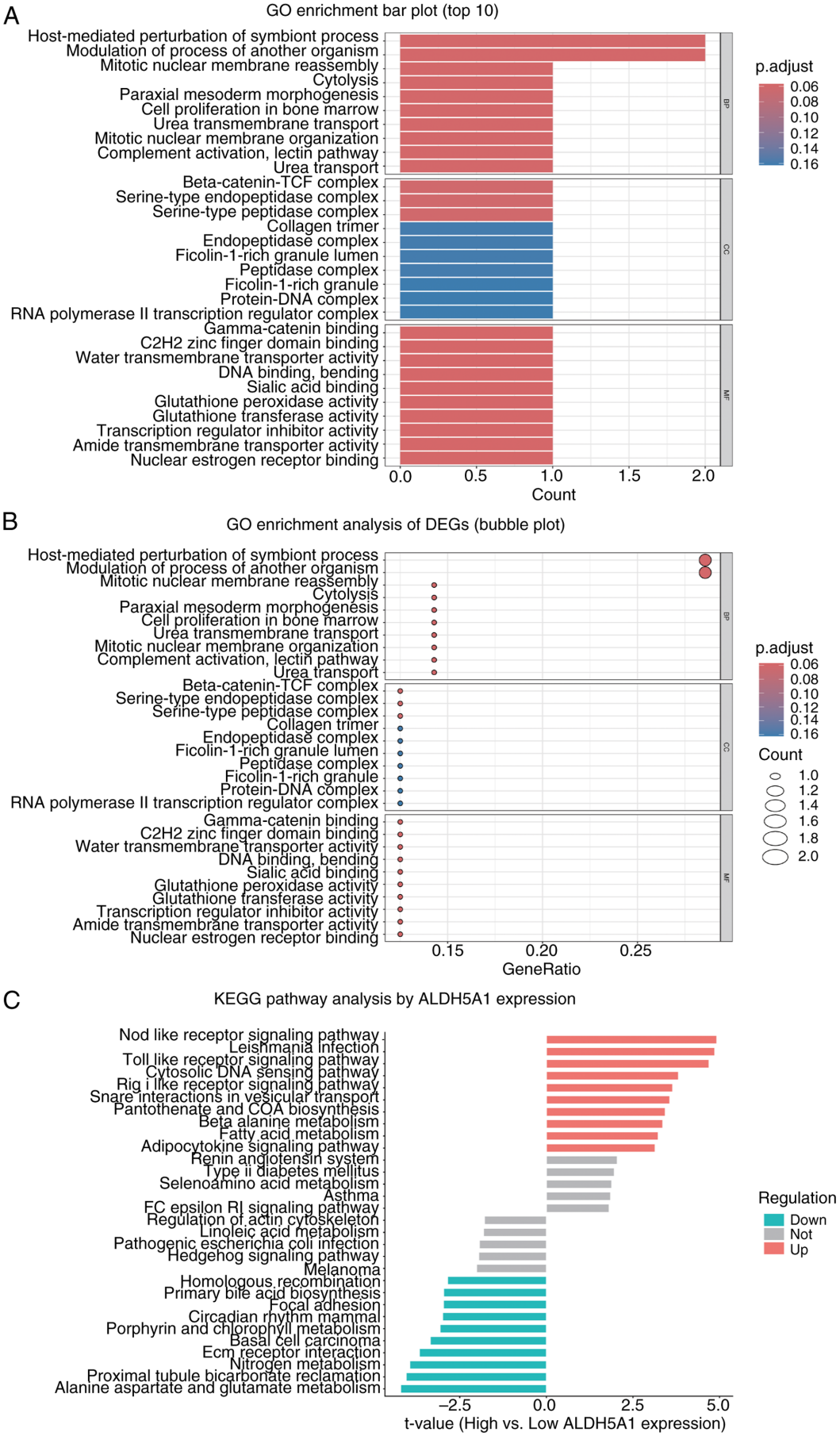

Figure 5. GO and GSVA enrichment analysis. (A) Bar plot of GO function enrichment analysis. (B) Bubble plot of GO enrichment analysis (C) GSVA analysis based on ALDH5A1 expression levels. GO, Gene Ontology; GSVA, Gene Set Variation Analysis; DEGs, differentially expressed genes; ALDH5A1, Aldehyde dehydrogenase 5 family member A1; KEGG, Kyoto Encyclopedia of Genes and Genomes.

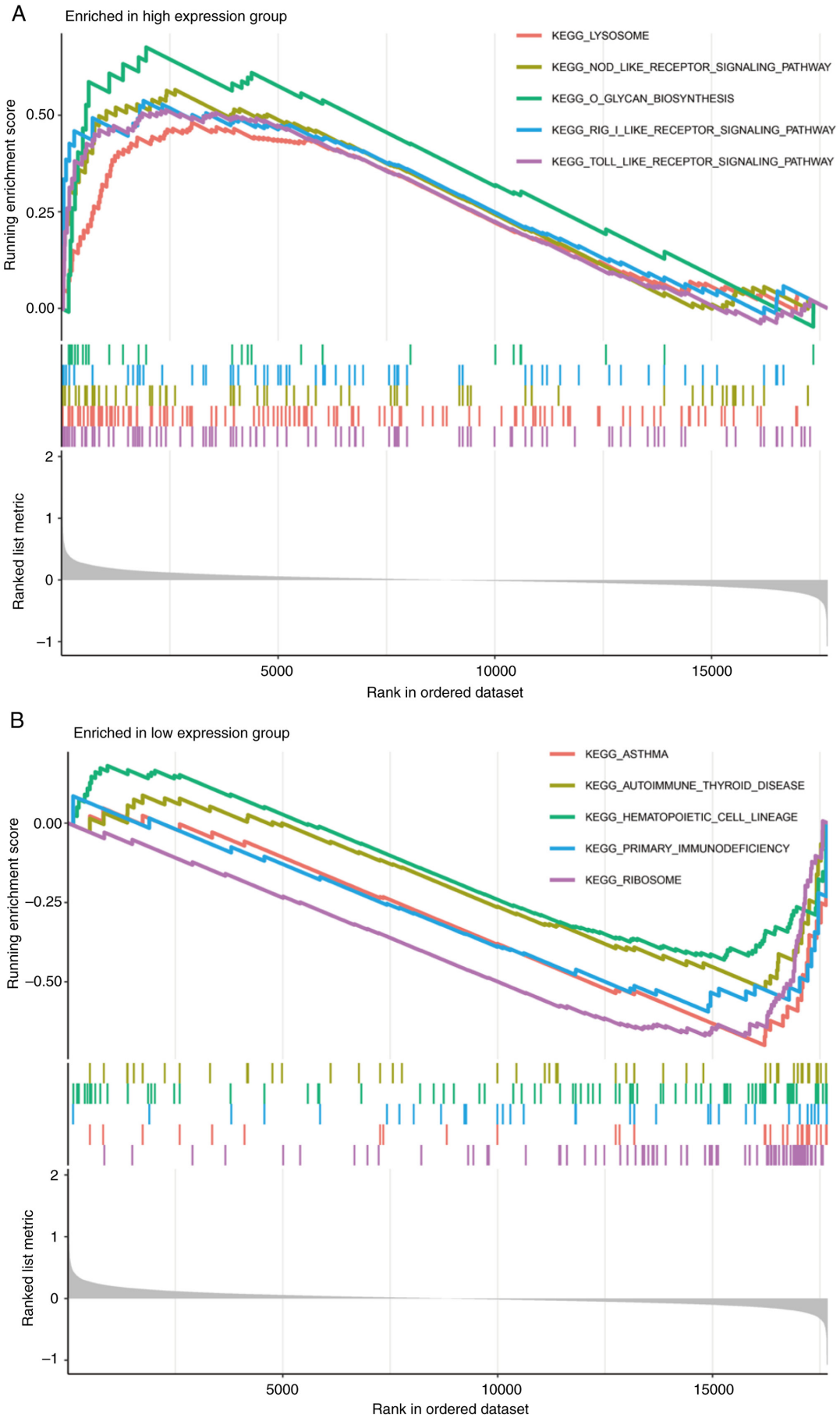

Figure 6. Gene set enrichment analysis. (A) Functional enrichment analysis of GSEA in the ALDH5A1 high expression group. (B) Functional enrichment analysis of GSEA in the ALDH5A1 low expression group. GSEA, Gene Set Enrichment Analysis; ALDH5A1, Aldehyde dehydrogenase 5 family member A1; KEGG, Kyoto Encyclopedia of Genes and Genomes.

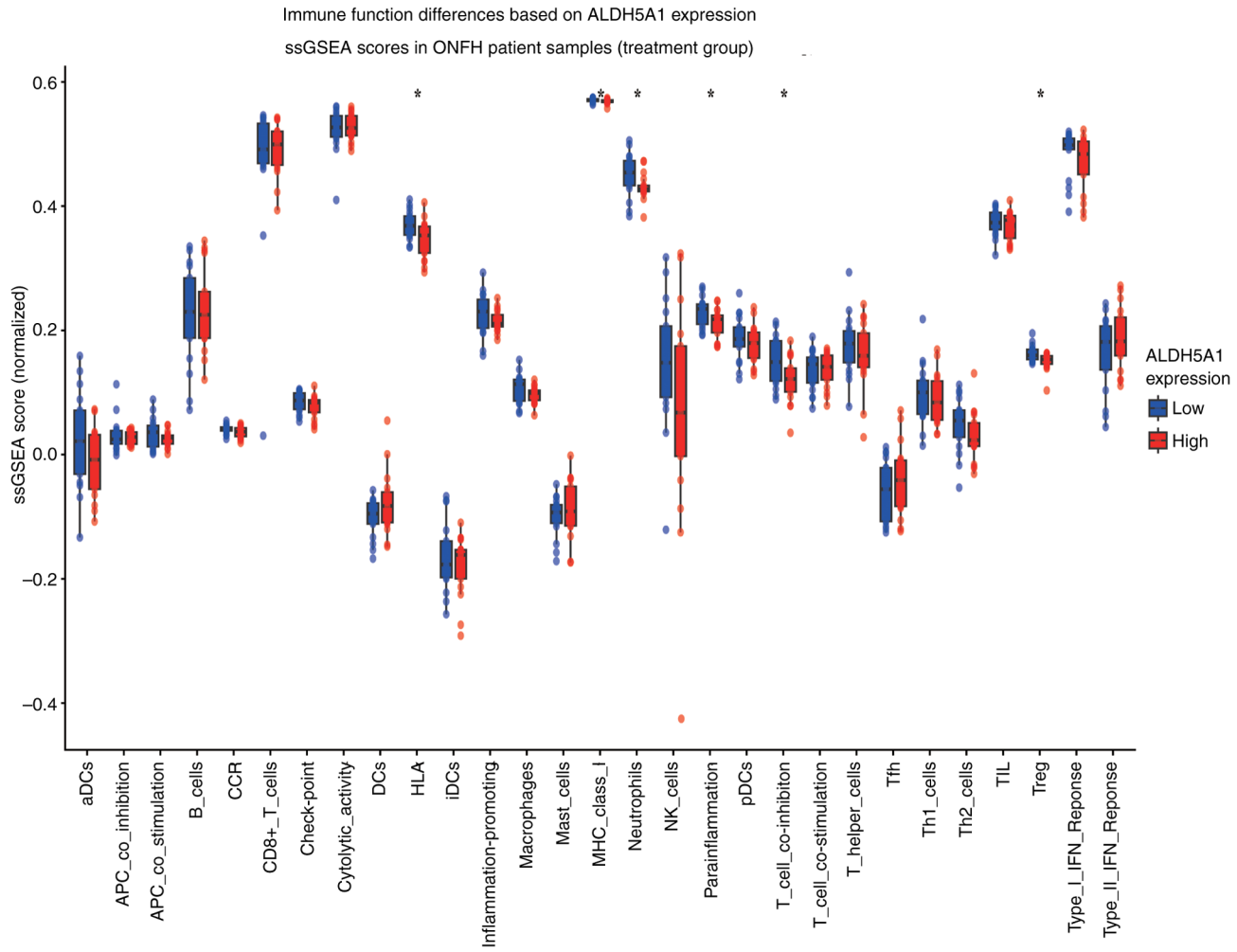

Figure 7. Differences in 29 immune-related functions across different ALDH5A1 expression levels. *P<0.05. ONFH, osteonecrosis of the femoral head; ssGSEA, single-sample Gene Set Enrichment Analysis; ALDH5A1, aldehyde dehydrogenase 5 family member A1.

between activated $CD4^+$ memory T cells and memory B cells, T cells, follicular helper cells, dendritic cells, and activated NK cells. Additionally, the lollipop plot (Fig. 9A) demonstrates a significant association (P<0.05) between immune cells and ALDH5A1, with the most notable finding being a negative correlation between ALDH5A1 and activated $CD4^+$ memory T cells (Fig. 9B). These results highlight the complex interactions between immune cells that contribute to ONFH progression and suggest that ALDH5A1 plays a key regulatory role in this immune network.

ceRNA network for detecting characteristic genes. LncRNAs have gained increasing attention in genetic research due to their substantial effects on various biological processes, including cellular regulation. Using three databases-TargetScan, miRanda, and miRDB-this study analyzed the regulatory interactions between ALDH5A1 and miRNAs. Our findings revealed 18 miRNAs that regulate ALDH5A1. Additionally, 68 lncRNAs that compete with these miRNAs for binding to MREs were identified (Fig. 10). These results suggest that ALDH5A1 regulates both its own expression and that of other molecular targets through the ceRNA network, which may play a pivotal role in the pathogenesis of avascular necrosis of the femoral head.

Bioinformatics and experimental analysis of ALDH5A1 expression. Bioinformatics analysis revealed a significant decrease in ALDH5A1 expression in chondrocytes from the ONFH group compared to the normal group (P<0.05). This was corroborated by qRT-PCR, which showed a marked reduction in ALDH5A1 mRNA levels in the ONFH group (Fig. 11A). Western blot analysis further confirmed that ALDH5A1 protein expression was significantly lower in the ONFH group than in the normal group (P<0.05) (Fig. 11B and C). Immunofluorescence staining also demonstrated reduced ALDH5A1 fluorescence intensity in the ONFH group relative to the normal group (Fig. 11D and E). The relative fluorescence intensity of ALDH5A1 in the ONFH group was significantly lower (P<0.01), providing additional support for the decreased ALDH5A1 expression in ONFH chondrocytes. These findings from bioinformatics, qRT-PCR, Western blot, and immunofluorescence analyses collectively confirm that ALDH5A1 expression is significantly reduced in ONFH samples compared to normal controls.

Discussion

ONFH is a complex, progressive disease primarily characterized by microcirculatory disorders and necrosis of

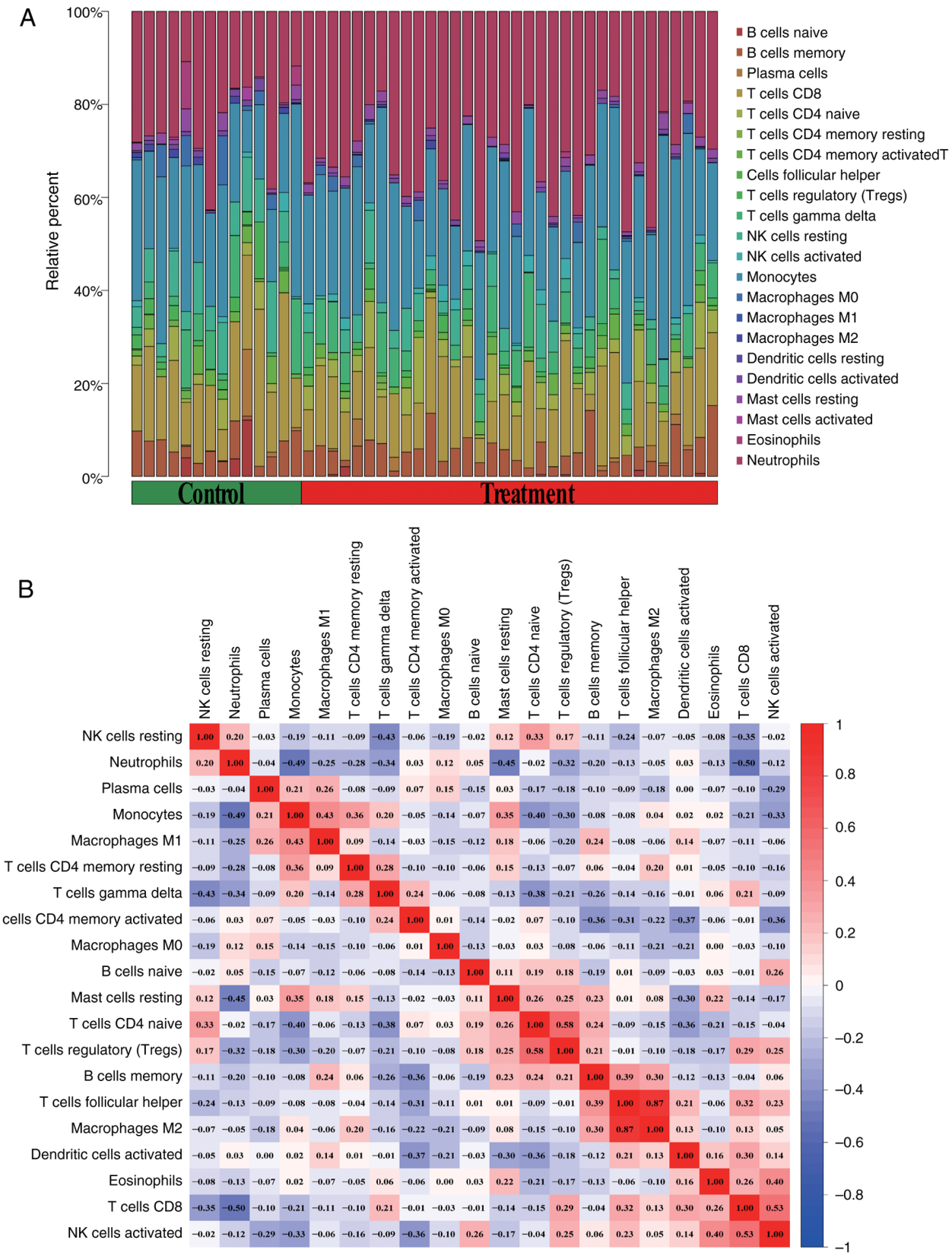

Figure 8. Immune cell infiltration analysis. (A) Stacked bar plot of immune cell infiltration (CIBERSORT) showing the relative percentage (Y-axis) of 22 immune cell types for each sample, grouped by Control (green) and ONFH (treatment, red). (B) Immune cell infiltration analysis volcano plot showing correlation between immune cells in the ONFH treatment group. ONFH, osteonecrosis of the femoral head.

bone marrow mesenchymal stem cells. Despite extensive research, the mechanisms underlying ONFH remain unclear, and the absence of reliable diagnostic markers often results in delayed treatment, eventually necessitating joint replacement (17). This study explores mRNA expression profiles in the peripheral blood serum of patients with ONFH and

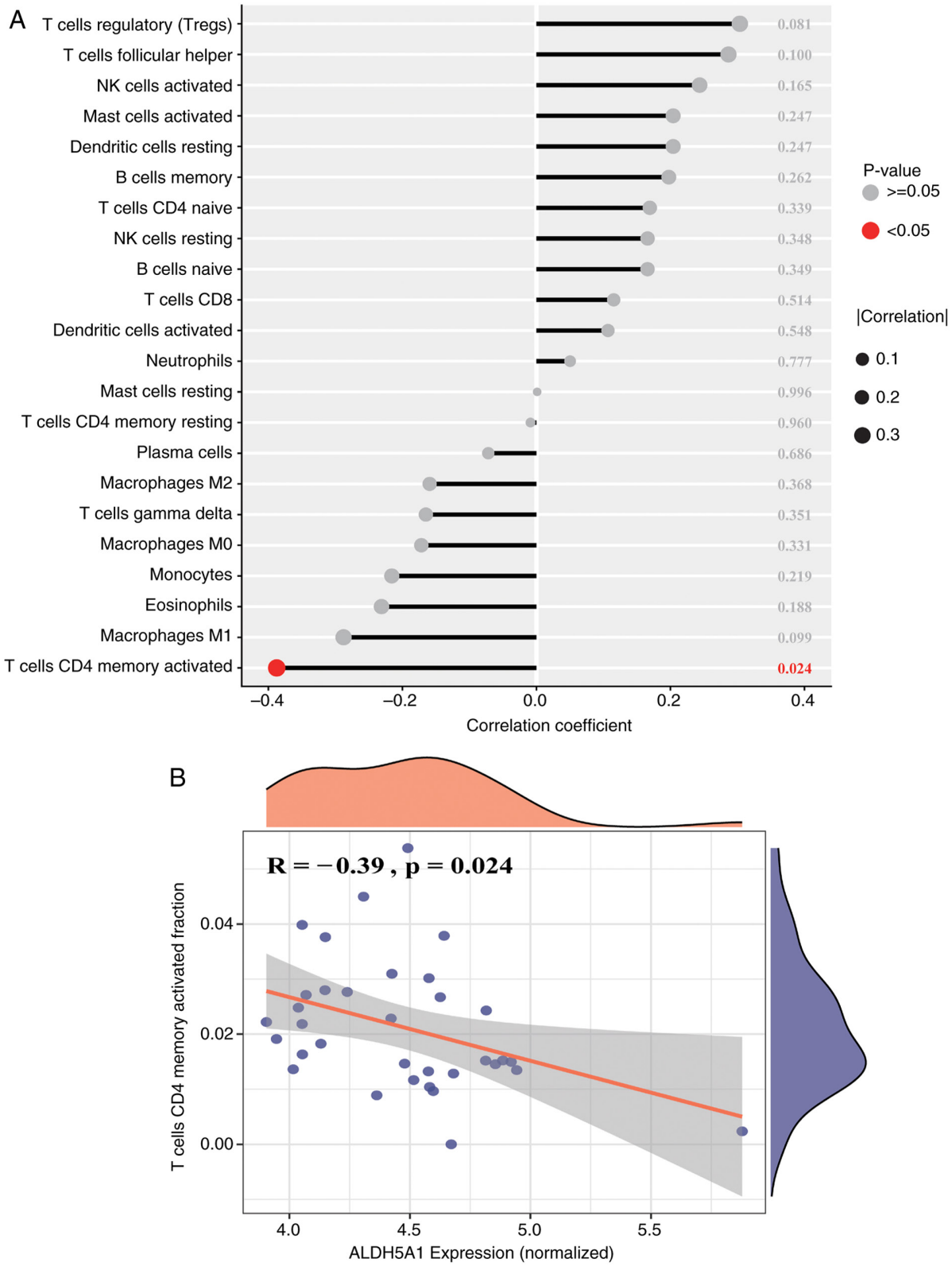

Figure 9. Immune correlation analysis. (A) Lollipop plot of correlations between ALDH5A1 expression and immune cell infiltration. The X-axis shows the Spearman correlation coefficient. The size of the circles corresponds to the absolute correlation coefficient (|Correlation|), and the color indicates statistical significance (Red for P<0.05, Grey for P≥0.05). The P-values are displayed on the right. (B) Distribution of Spearman correlation of activated CD4 memory T cells with ALDH5A1 in samples from patients with ONFH. ALDH5A1, Aldehyde dehydrogenase 5 family member A1; ONFH, osteonecrosis of the femoral head.

healthy controls, incorporating data from hip joint cartilage. Differential analysis and machine learning algorithms were employed to identify potential biomarkers, while the CIBERSORT algorithm was used to investigate correlations between immune cell populations and ONFH. Additionally, mRNA-miRNA-lncRNA relationships linked to key genes

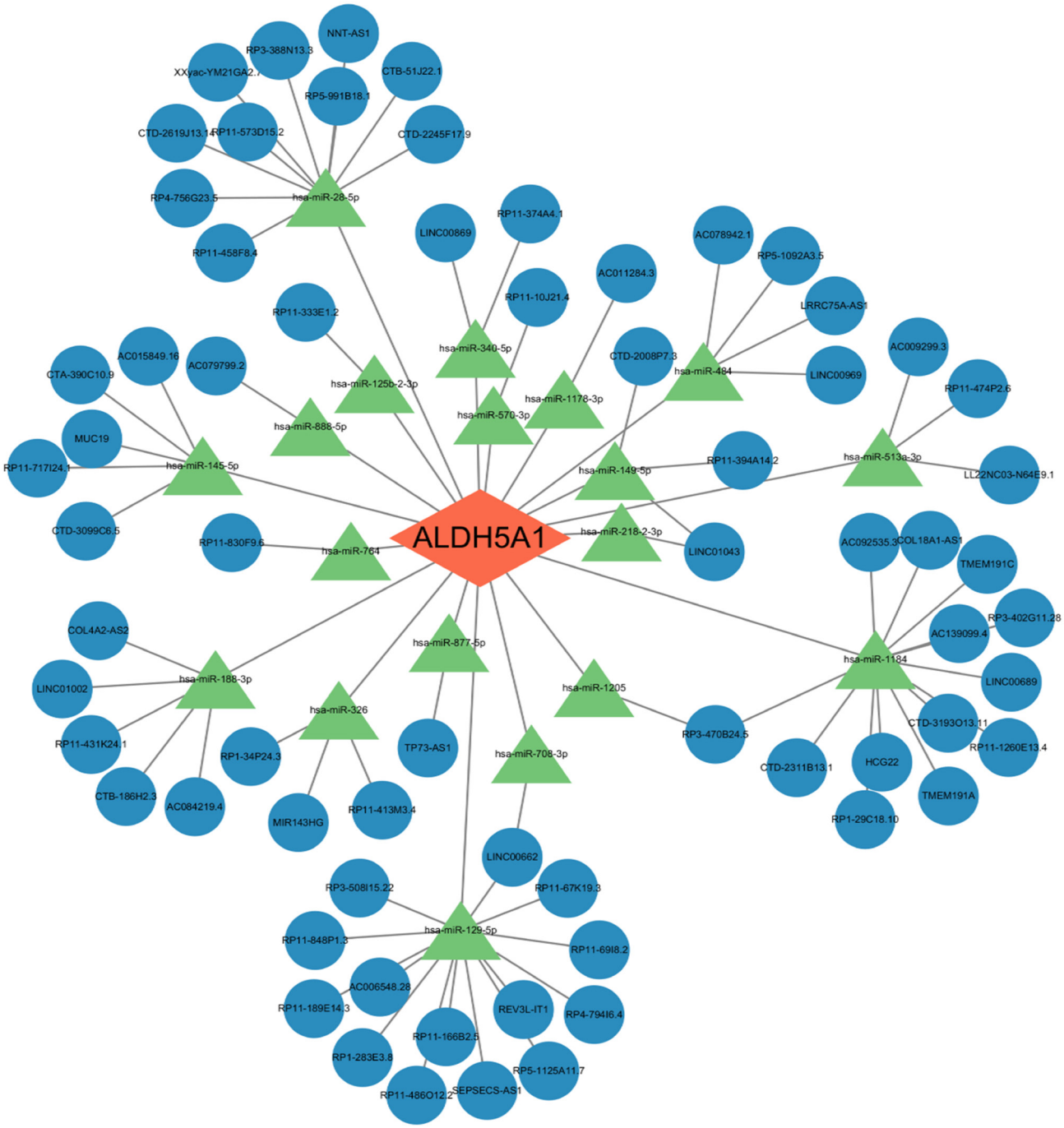

Figure 10. Plot of the competing endogenous RNA network of ALDH5A1. ALDH5A1, Aldehyde dehydrogenase 5 family member A1.

were predicted. The expression of hub genes was validated through qRT-PCR and Western blot, with results consistent with our bioinformatics analysis.

A bioinformatic analysis identified DEGs associated with ONFH. A total of 51 relevant genes were screened, including 18 upregulated and 33 downregulated genes, which may serve as significant biomarkers for the pathogenesis and progression of ONFH. Through methods such as LASSO regression, the SVM algorithm, and RF analysis, ALDH5A1, TBCEL, and KAT2B were identified as key genes. ALDH5A1 encodes succinate semialdehyde dehydrogenase, an enzyme involved in mitochondrial glutamate metabolism, regulating energy metabolism and maintaining mitochondrial integrity. Depletion of ALDH5A1 can result in mitochondrial dysfunction, impaired γ-aminobutyric acid (GABA) metabolism (18), and is associated with reduced ATP production, increased oxidative stress, and compromised mitochondrial dynamics, leading to cell apoptosis and inflammation (19). Following ischemic necrosis of the femoral head, an oxidative stress microenvironment develops in the necrotic bone area, driven by excessive reactive oxygen species (ROS) and apoptosis-inducing factors released from damaged mitochondria (20). While low levels of ROS participate in essential cellular signaling, excessive ROS production induces oxidative stress, disrupting cellular homeostasis and impairing function (21-23). ROS are also critical in activating autophagy and osteoblast apoptosis (24,25).

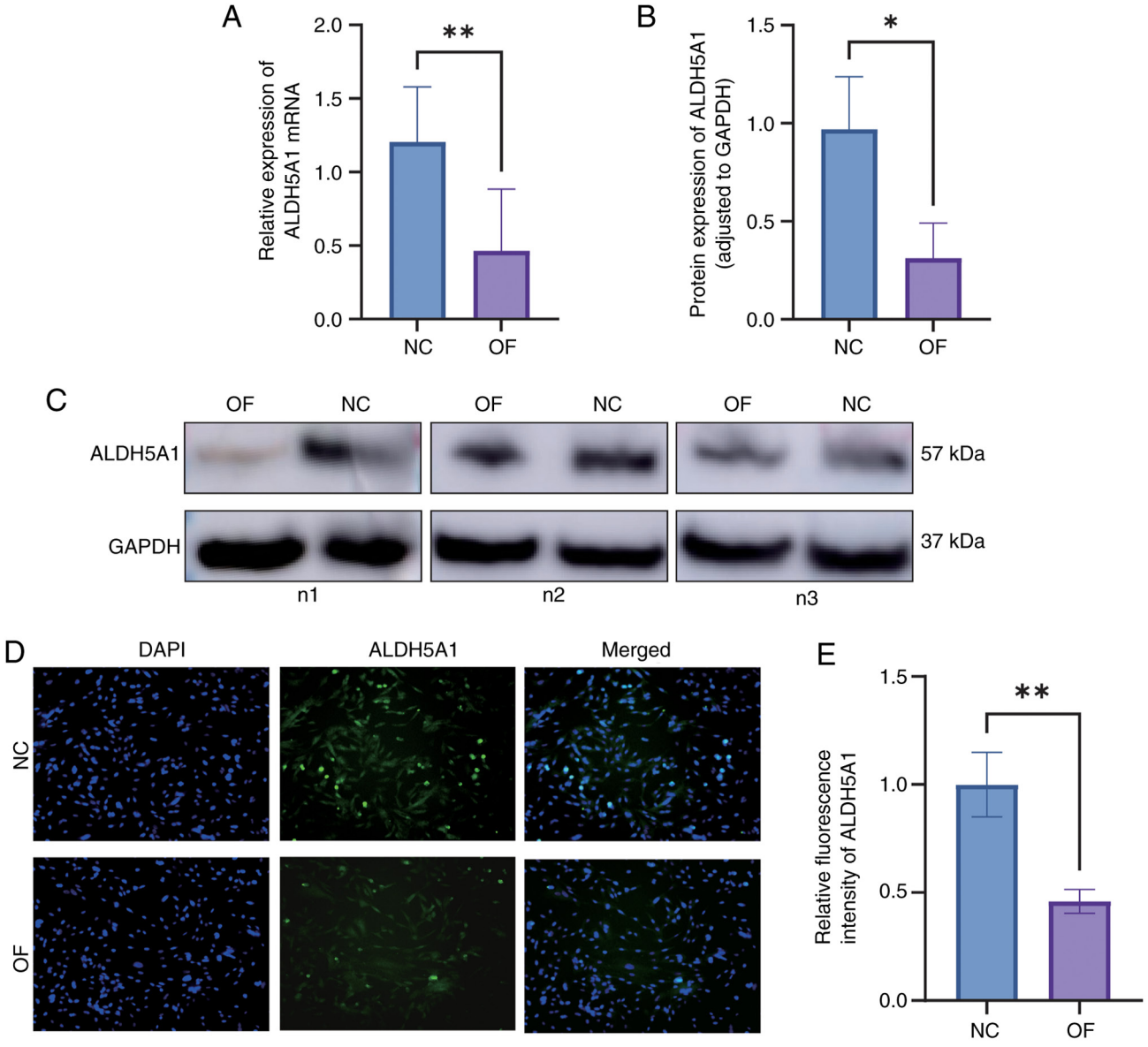

Figure 11. Verification of ALDH5A1 expression. (A) RT-qPCR analysis of ALDH5A1 mRNA levels in chondrocytes from the NC and ONFH groups. (B) Densitometric quantification of ALDH5A1 protein expression in the NC and ONFH groups. (C) Representative western blot images showing ALDH5A1 and the loading control GAPDH in the NC and ONFH groups (n=3). (D) Immunofluorescence staining of ALDH5A1 in chondrocytes from the NC and ONFH groups. ALDH5A1 is shown in green and nuclei are counterstained with DAPI (blue). (E) Quantification of the relative fluorescence intensity of ALDH5A1 in the NC and ONFH groups. *P<0.05 and **P<0.01. ALDH5A1, aldehyde dehydrogenase 5 family member A1; ONFH, osteonecrosis of the femoral head; NC, normal control.

Moreover, glucocorticoids, a major cause of non-traumatic ONFH, promote ROS production in osteoblasts, activating the JNK/c-Jun signaling pathway, which triggers autophagy and apoptosis (26). ROS inhibitors can reduce ROS levels, inhibit the JNK/c-Jun pathway, and reverse glucocorticoid-induced osteoblast apoptosis and autophagy (27). Furthermore, glucocorticoids impair cell angiogenesis, disrupt mitochondrial function, and hinder the blood supply to the femoral head, ultimately leading to bone necrosis (28).

Differential analysis of ALDH5A1 gene expression between the two groups revealed that its expression was significantly lower in the ONFH group compared to the normal group, further supporting our hypothesis. This suggests that ALDH5A1 may play a pivotal role in ONFH. To explore its potential function, the samples were divided into high and low ALDH5A1 expression groups, and enrichment analysis was performed on the DEGs. The GO results showed that the enriched genes were primarily involved in cellular autophagy, anion transmembrane transport, and proteasome-mediated ubiquitin-dependent protein catabolism. GSVA indicated that upregulated genes were enriched in pathways such as nitric oxide receptor signaling, Leishmania infection, TOLL-like receptor signaling, RIG-like receptor signaling, and vesicle transport-related interactions. These findings strongly implicate ALDH5A1-related DEGs in pathways like autophagy and lysosomal function, forming the basis for our mechanistic hypothesis. Although direct experimental validation of ALDH5A1's role in these specific pathways was not conducted in this study, the functional parallels with other members of the ALDH family provide substantial support for our hypothesis.

For instance, ALDH2, a well-characterized member of the family, protects against bone loss by regulating mitochondrial ROS and mitophagy, and modulates cell death pathways, including autophagy and ferroptosis, through detoxification of lipid peroxidation products. Additionally, other ALDH family members, such as ALDH1a3, sensitize cells to ferroptosis via autophagy-dependent ferritinophagy, while ALDH7A1 and ALDH3A1 act as inhibitors of ferroptosis (29,30). Although research on ALDH5A1 in these contexts is limited, the functional conservation observed across the ALDH family strengthens the plausibility of our findings. It is hypothesized that the downregulation of ALDH5A1 contributes to ONFH pathogenesis through mechanisms akin to its family members, such as impaired mitochondrial integrity, failure to detoxify ROS, and subsequent dysregulation of protective autophagy and ferroptosis pathways (31,32). This positions ALDH5A1 not only as a potential biomarker but also as a novel mechanistic component in ONFH pathology.

Our analysis also highlighted significant differences in immune cell functions, including HLA and T cell co-inhibition, between the high and low ALDH5A1 expression groups (9). Notably, ALDH5A1 expression was significantly negatively correlated with activated $CD4^+$ memory T cells (33), suggesting a potential link between ALDH5A1's metabolic role and the immune microenvironment in ONFH, which warrants further investigation (34). Finally, a predictive mRNA-miRNA-lncRNA ceRNA network was constructed, revealing complex upstream regulatory mechanisms for ALDH5A1 (Fig. 10). While this network is purely predictive, it provides a foundation for future studies on the regulation of ALDH5A1 in ONFH.

The identification of ALDH5A1 as a robust biomarker paves the way for several potential clinical applications. In diagnostic settings, ALDH5A1 expression, possibly measured in synovial fluid aspirates or synovial biopsies, could serve as an objective molecular marker, complementing standard imaging techniques. This could be particularly useful for diagnosing early-stage ONFH, even before significant radiographic changes are evident. Additionally, ALDH5A1 may prove valuable as a prognostic tool. It is hypothesized that its expression level at diagnosis could correlate with disease severity or progression. Specifically, markedly low ALDH5A1 levels may indicate a higher risk or faster progression to femoral head collapse, aiding in patient stratification for either joint-preserving procedures or total hip arthroplasty. While our study focused on tissue samples, future research should explore whether the ALDH5A1 protein or its downstream metabolites can be detected as a non-invasive blood biomarker, representing a significant advancement in ONFH management.

However, this study has several limitations. Firstly, a key limitation is the mismatch in tissue types between our discovery and validation cohorts. Our bioinformatics analysis was based on publicly available synovial tissue datasets, while experimental validation was conducted on articular cartilage. These tissues are histologically distinct. Our rationale is based on the premise that ONFH evolves into a 'whole-joint' disease, where secondary synovitis and cartilage degradation are linked by a shared microenvironment. While our data supports this hypothesis, this constitutes indirect validation. Future studies should confirm these findings in matched synovial, cartilage, and subchondral bone samples from the same patient cohort. Secondly, the sample size for our *in vitro* experimental validation was relatively small (n=6 per group), limiting the statistical power and reliability of our conclusions. Larger patient cohorts will be necessary to confirm our findings. Thirdly, the validated molecules have not yet been confirmed *in vivo*. Additional research is needed to validate the role of these molecules in ONFH *in vivo*.

In conclusion, this study used machine learning methods to identify ALDH5A1 as a key gene associated with ONFH, suggesting its potential as a prognostic marker. This finding was validated through ROC curves and *in vitro* experiments. Furthermore, significant correlations between key genes and immune cells were observed, and the ceRNA network relationships between miRNAs, lncRNAs, and hub genes were predicted. Our findings contribute to a deeper understanding of ONFH pathogenesis and provide potential molecular markers for the prognosis and treatment of the disease.

Acknowledgements

Not applicable.

Funding

This research was supported by the Guangxi Natural Science Foundation (grant no. 2023GXNSFAA026402), the Guangxi Medical and Health Appropriate Technology Development and Extension and Application Project (grant no. GZSY22-62), the Nanning Qingxiu District Science and Plan Project (grant no. 2020018), the Guangxi Science and Technology Base and Talent Special Project (grant no. GuikeAD19254003), and the Health Department of Guangxi Zhuang Autonomous Region Self-funded project (grant no. Z2013039).

Availability of data and materials

This study analyzed publicly available datasets, which can be accessed through the Gene Expression Omnibus (GEO) platform (https://www.ncbi.nlm.nih.gov/geo/). The data generated in this study can be requested from the corresponding author.

Authors' contributions

TR, QQ, LP, XZ, JH, JM, YQ, ZL and JY participated in conceptualizing the topic, designing the experimental study, implementing and analyzing data. TR, QQ, LP, XZ, JH, JM, YQ, ZL and JY acquired and interpreted graphs and figures, and drafted, revised and critically reviewed the article. All authors have read and approved the final manuscript, agreed to the journal for submission, and have accepted responsibility for all aspects of the work. TR and JY confirm the authenticity of all the raw data.

Ethics approval and consent to participate

The study was approved by the Medical Ethics Committee of the First Affiliated Hospital of Guangxi Medical University (approval no. 2021-E67-01). Written informed consent was

obtained from the participants at the time of tissue collection for the use of their discarded tissues in anonymized biomedical research. The consent form explicitly included permission for the use of any discarded pathological tissue for future research. The Ethics Committee confirmed that re-consent for the use of tissue in the present study was unnecessary, as the original consent was broad enough to cover retrospective research using these anonymized samples.

Patient consent for publication

Not applicable.

Competing interests

The authors have declared that they have no competing interests.

References

1. Zhao DW, Zhang F, Wang BJ, Liu BY, Li L, Kim SY, Goodman SB, Hernigou P, Cui Q, Lineaweaver WC, *et al*: Guidelines for clinical diagnosis and treatment of osteonecrosis of the femoral head in adults (2019 version). J Orthop Translat 21: 100-110, 2020.
2. Zhou W, Qu M, Lv YJ and Zhu JY: New advances in stem cell therapy for osteonecrosis of the femoral head. Curr Stem Cell Res Ther 14: 226-229, 2019.
3. Arbab D and König DP: Atraumatic femoral head necrosis in adults. Dtsch Arztebl Int 113: 31-38, 2016.
4. Cohen-Rosenblum A and Cui QJ: Osteonecrosis of the femoral head. Orthop Clin North Am 50: 139-149, 2019.
5. Migliorini F, Maffulli N, Baroncini A, Eschweiler J, Tingart M and Betsch M: Prognostic factors in the management of osteonecrosis of the femoral head: A systematic review. Surgeon 21: 85-98, 2023.
6. Sadile F, Bernasconi A, Russo S and Maffulli N: Core decompression versus other joint preserving treatments for osteonecrosis of the femoral head: A meta-analysis. Brit Med Bull 118: 33-49, 2016.
7. Cao HJ, Guan HF, Lai YX, Qin L and Wang XL: Review of various treatment options and potential therapies for osteonecrosis of the femoral head. J Orthop Translat 4: 57-70, 2015.
8. Mont MA, Salem HS, Piuzzi NS, Goodman SB and Jones LC: Nontraumatic osteonecrosis of the femoral head: Where do we stand today?: A 5-year update. J Bone Joint Surg Am 102: 1084-1099, 2020.
9. Yu R, Zhang J, Zhuo Y, Hong X, Ye J, Tang S, Liu N and Zhang Y: ARG2, MAP4K5 and TSTA3 as diagnostic markers of steroid-induced osteonecrosis of the femoral head and their correlation with immune infiltration. Front Genet 12: 691465, 2021.
10. Fang W, Peng P, Lin K, Xiao F, He W, He M and Wei Q: m6A methylation modification and immune infiltration analysis in osteonecrosis of the femoral head. J Orthop Surg Res 19: 183, 2024.
11. Rodriques SG, Stickels RR, Goeva A, Martin CA, Murray E, Vanderburg CR, Welch J, Chen LM, Chen F and Macosko EZ: Slide-seq: A scalable technology for measuring genome-wide expression at high spatial resolution. Science 363: 1463-1467, 2019.
12. Chen B, Khodadoust MS, Liu CL, Newman AM and Alizadeh AA: Profiling tumor infiltrating immune cells with CIBERSORT. Methods Mol Biol 1711: 243-259, 2018.
13. Shi Y, Yang F, Wei S and Xu G: Identification of key genes affecting results of hyperthermia in osteosarcoma based on integrative ChIP-Seq/TargetScan analysis. Med Sci Monitor 23: 2042-1048, 2017.
14. John B, Enright AJ, Aravin A, Tuschl T, Sander C and Marks DS: Human MicroRNA targets. PLoS Biol 2: e363, 2004.
15. Chen YH and Wang XW: miRDB: An online database for prediction of functional microRNA targets. Nucleic Acids Res 48: D127-D131, 2020.
16. Yang Q, Zhang P, Han L, Shi PS, Zhao ZF, Cui DJ and Hong K: Mitochondrial-related genes PDK2, CHDH, and ALDH5A1 served as a diagnostic signature and correlated with immune cell infiltration in ulcerative colitis. Aging (Albany NY) 16: 3803-3822, 2024.
17. Song Y, Du ZW, Yang QW, Ren M, Wang QY, Wang A, Chen GY, Zhao HY, Yu T and Zhang GZ: Association of genes variants in RANKL/RANK/OPG signaling pathway with the development of osteonecrosis of the femoral head in Chinese population. Int J Med Sci 14: 690-697, 2017.
18. Kim KJ, Pearl PL, Jensen K, Snead OC, Malaspina P, Jakobs C and Gibson KM: Succinic semialdehyde dehydrogenase: Biochemical-molecular-clinical disease mechanisms, redox regulation, and functional significance. Antioxid Redox Signal 15: 691-718, 2011.
19. Jackson B, Brocker C, Thompson DC, Black W, Vasiliou K, Nebert DW and Vasiliou V: Update on the aldehyde dehydrogenase gene (ALDH) superfamily. Hum Genomics 5: 283-303, 2011.
20. Brown MN, Gibson KM, Schmidt MA, Walters DC, Arning E, Bottiglieri T and Roullet JB: Cellular and molecular outcomes of glutamine supplementation in the brain of succinic semialdehyde dehydrogenase-deficient mice. JIMD Rep 56: 58-69, 2020.
21. Hu XF, Wang L, Xiang G, Lei W and Feng YF: Angiogenesis impairment by the NADPH oxidase-triggered oxidative stress at the bone-implant interface: Critical mechanisms and therapeutic targets for implant failure under hyperglycemic conditions in diabetes. Acta Biomater 73: 470-487, 2018.
22. McGarry T, Biniecka M, Veale DJ and Fearon U: Hypoxia, oxidative stress and inflammation. Free Radic Biol Med 125: 15-24, 2018.
23. Wauquier F, Leotoing L, Coxam V, Guicheux J and Wittrant Y: Oxidative stress in bone remodelling and disease. Trends Mol Med 15: 468-477, 2009.
24. Shadel GS and Horvath TL: Mitochondrial ROS signaling in organismal homeostasis. Cell 163: 560-569, 2015.
25. Volpe CMO, Villar-Delfino PH, dos Anjos PMF and Nogueira-Machado JA: Cellular death, reactive oxygen species (ROS) and diabetic complications. Cell Death Dis 9: 119, 2018.
26. De Meyer GRY, De Keulenaer GW and Martinet W: Role of autophagy in heart failure associated with aging. Heart Fail Rev 15: 423-430, 2010.
27. Assouline-Dayan Y, Chang C, Greenspan A, Shoenfeld Y and Gershwin ME: Pathogenesis and natural history of osteonecrosis. Semin Arthritis Rheu 32: 94-124, 2002.
28. Peng PJ, Nie ZG, Sun F and Peng H: Glucocorticoids induce femoral head necrosis in rats through the ROS/JNK/c-Jun pathway. FEBS Open Bio 11: 312-321, 2021.
29. Yao X, Yu S, Jing X, Guo J, Sun K, Guo F and Ye Y: PTEN inhibitor VO-OHpic attenuates GC-associated endothelial progenitor cell dysfunction and osteonecrosis of the femoral head via activating Nrf2 signaling and inhibiting mitochondrial apoptosis pathway. Stem Cell Res Ther 11: 140, 2020.
30. Shidoji Y, Hayashi K, Komura S, Ohishi N and Yagi K: Loss of molecular interaction between cytochrome c and cardiolipin due to lipid peroxidation. Biochem Biophys Res Commun 264: 343-347, 1999.
31. Li J, Cao F, Yin HL, Huang ZJ, Lin ZT, Mao N, Sun B and Wang G: Ferroptosis: Past, present and future. Cell Death Dis 11: 88, 2020.
32. Su LJ, Zhang JH, Gomez H, Murugan R, Hong X, Xu DX, Jiang F and Peng ZY: Reactive oxygen species-induced lipid peroxidation in apoptosis, autophagy, and ferroptosis. Oxid Med Cell Longev 2019: 5080843, 2019.
33. Chen C, Zhao X, Luo Y, Li B, Li Q, Zhao C, Huang Y and Kang P: Imbalanced T-cell subsets may facilitate the occurrence of osteonecrosis of the femoral head. J Inflamm Res 15: 4159-4169, 2022.
34. Chen X, Li J, Kang R, Klionsky D and Tang D: Ferroptosis: Machinery and regulation. Autophagy 17: 2054-2081, 2021.